



Experimental Study of Open Channel Model of Glass Fiber Reinforced Polymer and Its Flowing Characteristics

S. Hasyim^{a*}, N. Salam^b, M. Saleh Pallu^a, F. Maricar^a

^a Civil Engineering Department, Faculty of Engineering, Hasanuddin University, Gowa, South Sulawesi Province, Indonesia

^b Mechanical Engineering Department, Faculty of Engineering, Hasanuddin University, Gowa, South Sulawesi Province, Indonesia

PAPER INFO

Paper history:

Received 01 August 2023

Received in revised form 06 November 2023

Accepted 10 November 2023

Keywords:

Glass Fiber Reinforced Polymer

Open Channel Flume

Experimental Model

Manning Roughness Coefficient

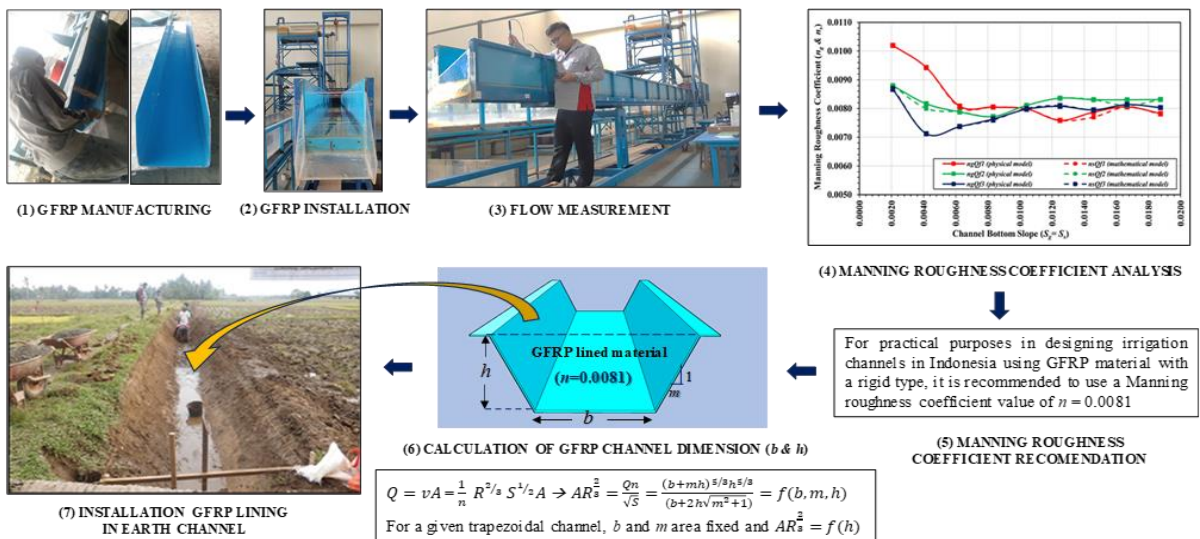
Nash-Sutcliffe Efficiency

ABSTRACT

One of the efforts to reduce water losses in irrigation channels is to provide lined materials in the earth's irrigation channels. Construction of these lined materials in Indonesia requires raw materials (such as sand, gravel, and split stone) mined from nature, and in Indonesia, known as class C excavated materials. Excessive exploitation of class C excavated materials will impact environmental damage. To overcome these problems, therefore, research is needed to find alternative lined materials, and in this research, the alternative lined material is Glass Fiber Reinforced Polymer (GFRP). The study's primary objective was to determine the value of the Manning roughness coefficient for lined channels made of GFRP material. The research involved experimental testing using an open channel model (flume) lined with GFRP material. The flow tests were conducted with three variations of the pump flow discharge and nine variations of the channel bottom slope. The test results from the physical model were compared with the results of the mathematical model simulation using the HEC-RAS software. The model's performance was evaluated using the graphical technique and quantitative statistics specifically the Nash-Sutcliffe Efficiency (NSE) method. Model evaluation with the NSE method shows that the performance of the physical model is "very good". The Manning roughness coefficient value for rigid-lined GFRP material range from 0.0071 to 0.0102. The recommended Manning roughness coefficient value for practical application in the design of irrigation channels in Indonesia is 0.0081.

doi: 10.5829/ije.2024.37.04a.10

Graphical Abstract



*Corresponding Author Email: suryadhs@yahoo.com (S. Hasyim)

1. INTRODUCTION

One of the efforts to increase the availability of irrigation water is to provide lining for earth irrigation channels so that this will have an impact on reducing the rate of water loss in irrigation channels. Based on Indonesian Irrigation Planning Standards, four types of materials are recommended for use as a lining in irrigation channels in Indonesia, such as stone masonry, concrete, soil-cement, and ferrocement. For irrigation channel planning in Indonesia, the Manning roughness coefficient (n) values recommended for use for the four types of lined material are respectively 0.0167, 0.0143, 0.0285 – 0.0222, and 0.0143 (1). Of the four types of lining, only two are the most widely used as lined material in irrigation channels in Indonesia, such as stone masonry lining and concrete lining. Apart from using a mixture of water and cement, the process for construction implementation of two types of lined materials also requires other raw materials such as sand, gravel, and crushed stone, mined from nature, and in Indonesia are known as class C excavated materials. The excessive exploitation of class C excavated materials will impact environmental damage, so it needs to be mitigated (2-4). In practice, also in the project site, the process of making the mixture for the lining of the channels from the stone masonry and concrete has several constraints, such as the difficulty of obtaining class C excavated material sources, the problematic access constraints to transport the mixed material constituents to the work location, the difficulty of obtaining fresh-water that is required for the process of mixing materials in the project site, and the difficulty of controlling the quality of the construction work due to the wide spread of the work locations (5). Figure 1 shows a case example of difficult access conditions for making concrete mixes for tertiary irrigation channel work at the Batang Anai Irrigation Project in West Sumatra Province, Indonesia, which was implemented in 2016.

From these problems, the preliminary research idea arose to find and study alternative materials that do not use cement and class C excavated materials.

One of the products of processed polymer materials is the geomembrane. Geomembrane as a lined channel



Figure 1. Construction of concrete lining on tertiary irrigation channels in the Batang Anai Irrigation Project in West Sumatra Province

material has been widely used in various countries. In the United States, geomembrane has been used as a lined material (membrane) in channels that control seepage since 1950s. It is an effective alternative material to replace traditional standard linings methods, such as concrete and compacted soil. One of the first uses of geomembranes for channels was in 1954 in irrigation channels by the U.S. Bureau of Reclamation (USBR) in Fort Collins, Colorado. USBR has extensive experience in geomembrane installation and monitoring for lined channels based on past field testing programs. PVC geomembrane was originally a geomembrane used for lined channels. However, subsequently, Polyethylene (PE) based geomembranes (such as HDPE, LDPE, CSPE, and VLDPE) and several other types of geomembranes (such as EDPM and Polypropylene) are also used as lined channels (6-8). In Portugal, prefabricated membranes for lined channel use are also increasing, especially as a solution for rehabilitating existing concrete channels. The two main types of membranes used in Portugal are bituminous membranes (modified bitumen polymers) and synthetic membranes (PVC) (9).

One of the most essential purposes of scientific research is finding new engineering composites that combine strength and lightweight (10). Polymer matrix composites are used in different industrial applications due to their enhanced mechanical properties and lightweight (11). Fiber-reinforced polymer (FRP) composites have better fatigue and corrosion-resistive performance than metals, reducing the maintenance cost (12). FRP is a composite material made of a polymer matrix reinforced with fibers. The fibers are usually glass, carbon, or aramid. The polymer is usually epoxy, vinyl ester, or polyester thermosetting plastic (13). Because of cost, glass, and carbon are the most widely used reinforcement materials for civil infrastructure composite applications. For applications that require large amounts of materials, glass is the most popular because it is the least expensive (14). The economic analysis indicated that glass fiber is more cost-benefit than carbon fiber in improving the concrete properties, especially for one layer of FRP (15). Polyesters are the most widely used polymers in FRP components for construction/civil infrastructure applications due to their relatively low cost and ease of processing (16). Polyester resins have many advantages, such as suitable adhesive and mechanical properties, better resistance to fatigue and micro cracking, reduced degradation from water ingress, increased resistance to osmosis (surface degradation due to water permeability), and good performance at elevated temperatures (17). Various fabrication techniques, such as hand layup, spray-up, filament winding, lamination, and pultrusion, are used to process polymeric composites (18).

Nowadays, Glass Fiber Reinforced Polymer (GFRP) composites are alternative products for metals due to their superior characteristics like high specific stiffness, corrosion resistance, fatigue resistance, and less weight-to-strength ratio (19). In Indonesia, GFRP materials are currently widely used as building materials in the construction industry. GFRP material generally has strong, lightweight, weather-resistant, and impermeable characteristics, so it is often used as a component of hydraulic structures (such as sliding gates, flap gates, and culverts) in swamp irrigation channels where the water conditions are acidic (Figure 2).

In order to design an irrigation channel using GFRP material lining, it is necessary to know the value of the hydraulic roughness coefficient first. GFRP material is currently also widely used in the manufacture of commercial piping products in various countries. Some of the piping products in the world that have included the value of the hydraulic roughness coefficient in their GFRP piping product specifications include the following:

1. Grandpipe®, a GFRP pipe manufacturing company from Turkey, gives a Manning roughness coefficient $n = 0.009$ for pipe material products called GRP (Glass-Reinforced Plastics)¹.
2. Jiubo Composite®, a GFRP pipe manufacturing company from China, gives a Manning roughness coefficient $n = 0.0084$ for pipe material products called FRP (Fiber-Reinforced Plastics)².

There is still little research using GFRP-lined material in open channels like irrigation channels. In 1975, Malaysia conducted trials on using GFRP material as a lined material in a pilot project for constructing a new tertiary irrigation channel implemented at the Tanjung Karang Irrigation Project. The construction of the tertiary irrigation channels was a typical flume-shape with the characteristics of a rigid GFRP material and was named Fiberglass-Reinforced Polyester (FRP) (20). Japan had also implemented using materials made from GFRP as lined materials to repair existing concrete lining in irrigation channels that had minor cracks. The material lining made of GFRP has flexible characteristics and is



Figure 2. Example of using GFRP flap gates in swamp irrigation channels in Central Kalimantan Province, Indonesia

named FFRP (Flexible Fiber Reinforced Plastic). Some samples of the FFRP material were taken to the laboratory to be tested experimentally using an open channel model of a rectangular flume to examine the value of the hydraulic roughness coefficient. The results of their research found that the Manning roughness coefficient is $n = 0.0094$ (21). Since the idea of using lining with GFRP material in Indonesia is to line earth irrigation channels, the characteristics of the GFRP material must be rigid. Based on this explanation, the final idea of the research was to find the value of the hydraulic roughness coefficient for GFRP material with a rigid type produced by a factory in Indonesia. The primary objectives of the study include:

1. To evaluate the effects of discharge and channel bottom slope changes on flow velocity and flow depth characteristics.
2. To analyze the impact of changes in discharge and channel bottom slope on the value of the Manning roughness coefficient and to interpret the range of Manning roughness coefficient values obtained from the test results.
3. To propose the recommended Manning roughness coefficient value for GFRP material to be used in the design of irrigation channels in Indonesia.

After the innovative value for the Manning roughness coefficient (n) for GFRP material resulting from this research has been obtained, the design of irrigation channel dimensions using GFRP lined material can be calculated using the uniform flow formula. Manning's formula and the continuity equation, $Q = Av$, form the basic equations for uniform-flow computation. The discharge Q is given as (22, 23):

$$Q = \frac{1}{n} AR^{2/3} S^{1/2} \quad (1)$$

$$Q = K\sqrt{S} \quad (2)$$

where,

Q	=	discharge (m ³ /s)
A	=	wetted area (m ²)
v	=	flow velocity (m/s)
n	=	Manning roughness coefficient
$R = A/P$	=	hydraulic radius (m)
P	=	wetted perimeter (m)
S	=	channel bottom slope

$K = \frac{1}{n} AR^{2/3}$ is called the channel's conveyance and expresses the channel's discharge capacity per unit longitudinal slope. For a given channel, $AR^{2/3}$ is a function of the flow depth. For example, in Figure 3 consider a trapezoidal section of bottom width = b and side slope m horizontal: 1 vertical.

¹ <https://grandpipe.com/en/product-information>

² <https://www.aldfpr.com/News/Comparison-of-FRP-Pipe-and-pipe-flow-185.html>

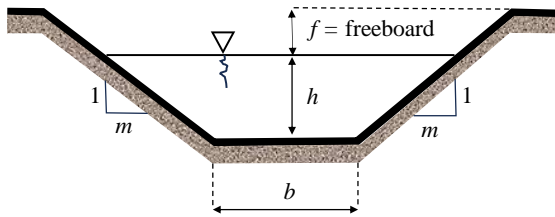


Figure 3. Hydraulic parameters on a trapezoidal channel cross section

Then,

$$A = (b + mh)h \quad (3)$$

$$P = (b + 2h\sqrt{m^2 + 1}) \quad (4)$$

$$R = \frac{A}{P} = \frac{(b+mh)h}{(b+2h\sqrt{m^2+1})} \quad (5)$$

$$AR^{\frac{2}{3}} = \frac{Qn}{\sqrt{S}} = \frac{(b+mh)^{5/3}h^{5/3}}{(b+2h\sqrt{m^2+1})} = f(b, m, h) \quad (6)$$

For a given trapezoidal channel, b and m are fixed and $AR^{\frac{2}{3}} = f(h)$. Since $AR^{\frac{2}{3}} = \frac{Qn}{\sqrt{S}}$, and if Manning roughness coefficient (n) and channel bottom slope (S) are fixed for a channel, the channel have unique depth in uniform flow associated with each discharge. The depth is called the normal depth (h).

After this innovative value for the Manning roughness coefficient has been obtained, the advantages that can be obtained from its application in irrigation channels are as follows:

1. The use of GFRP material can reduce the use of class C excavated materials in Indonesia so that the impact of environmental damage can be mitigated.
2. The process of making GFRP material segments can be carried out first in the factory so that it will reduce the constraints, such as the difficulty of obtaining class C excavated material sources, the problematic access constraints to transport the mixed material constituents to the work location, the difficulty of obtaining fresh-water that is required for the process of mixing materials on the project site, and the difficulty of controlling the quality of the construction work.
3. Because the weight of the GFRP material is relatively light, transporting the material to the work location will be cheaper.
4. Because the GFRP material structure design has been created, installing GFRP-lined material segments in earth irrigation channels will be carried out more effectively and efficiently (see Figure 4).

2. MATERIAL AND METHOD

The Experimental research conducted at the Hydraulics Laboratory, Civil Engineering Department, Faculty of

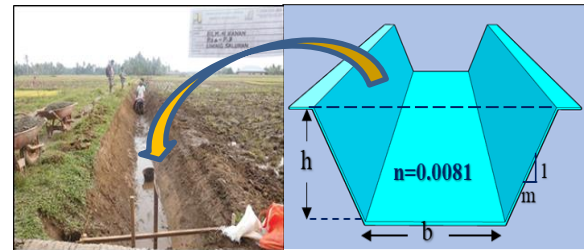


Figure 4. Illustration of installing GFRP material segment in an earth irrigation channel

Engineering, Hasanuddin University, South Sulawesi Province, Indonesia. The physical modeling used three pump discharge (Q_f) variations as input data flowed into the GFRP flume. The three variations of pump discharge (Q_f) are low inflow discharge (Q_{f1}), medium inflow discharge (Q_{f2}), and high inflow discharge (Q_{f3}). The GFRP flume bottom slopes (S_g) were also set for nine variations of channel bottom slopes, ranging from S_{g1} to S_{g9} .

2. 1. Material and Equipment

The primary material used in this study is GFRP (Glass Fiber Reinforced Polymer), produced by one of the factories in Indonesia. As a preliminary stage, measurements, manufacturing, packaging, and installation of the GFRP material into the flume were carried out, as shown in Figure 5.

The equipment used for experimental testing was as follows: a) an open channel (flume) model device lined with GFRP material; b) two submersible water pumps equipped with a pipe network and discharge control valves; c) a flow meter; d) water weighing scale; e) a point gauge; f) The flume's slope adjuster, as shown in Figure 6.

Precisely using this equipment during the experimental testing process is crucial to minimize errors in the hydraulic laboratory. Flow velocity was measured using a mini flow-meter because it can measure at a relatively low flow depth. Flow velocity and flow depth measurements can be seen in Figure 7.



Figure 5. (a) Measurements, (b) manufacturing, (c) packaging, and (d) installation of the GFRP material into the flume

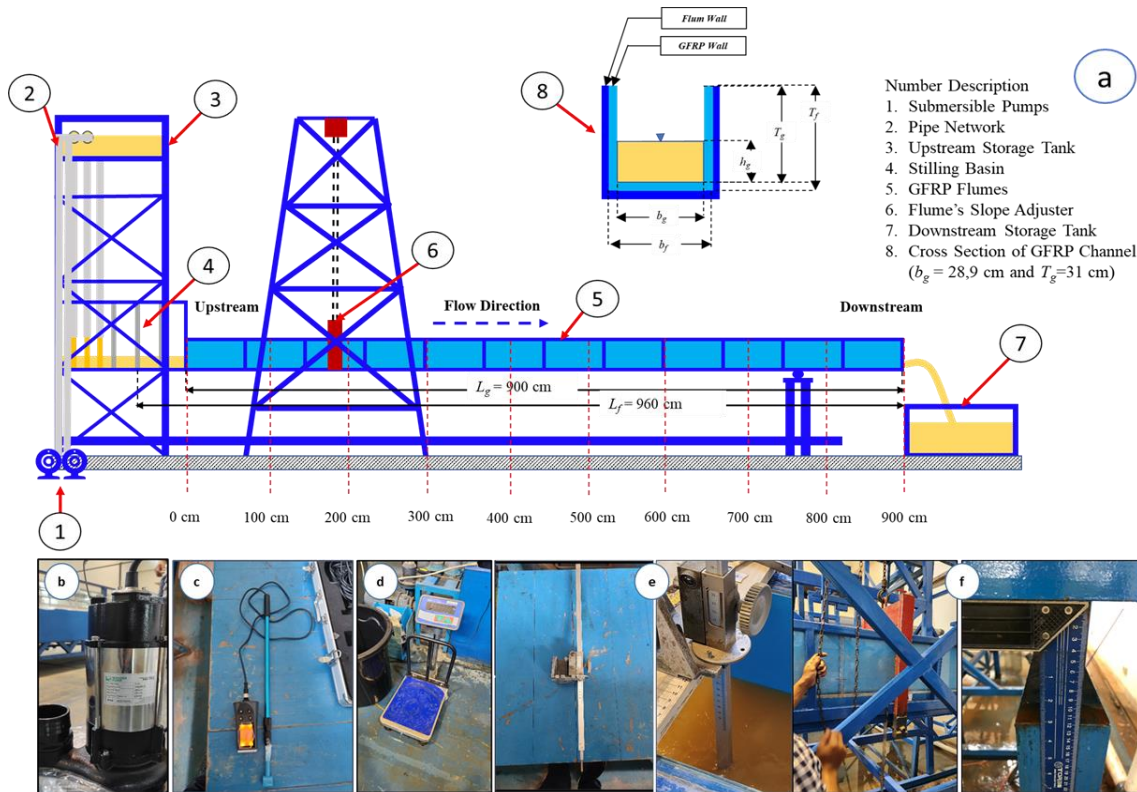


Figure 6. The flume model equipment and other devices used for experimental testing



Figure 7. (a) Flow velocity measurement using a flow meter (left) and (b) flow depth measurement using a point gauge (right)

2.2. Experimental Test Method The method used to obtain the Manning roughness coefficient value for GFRP material is by referring to the experimental test method carried out by Mera and Robi (24). They had carried out experimental tests to obtain the Manning coefficient value for PVC (Polyvinyl Chloride) material produced by a commercial company in Indonesia. The research was carried out using a flume device in the hydraulic laboratory at Andalas University in Padang City, West Sumatra Province, Indonesia. Experimental test was carried out using one flow discharge and ten variations of channel bottom slopes. From the implementation of their research, several results were obtained as follows:

1. Graph of the relationship between flow depth and variations in channel bottom slope (Figure 8);
2. Graph of the relationship between the Manning roughness coefficient and variations in channel bottom slopes (Figure 9);
3. From the Figure 9 graph, the Manning roughness coefficient value for PVC material obtained from the results of their research is in the range $n = 0.010$ to 0.014 .

The graph obtained from their research results (25) will later be compared with the graph obtained from this research to verify the accuracy of the proposed method.

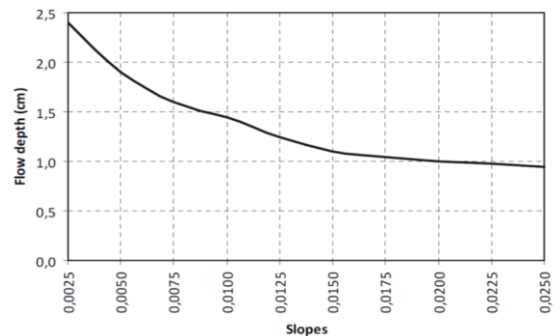


Figure 8. Graph of the relationship between flow depth and variations in channel bottom slope for PVC material (25)

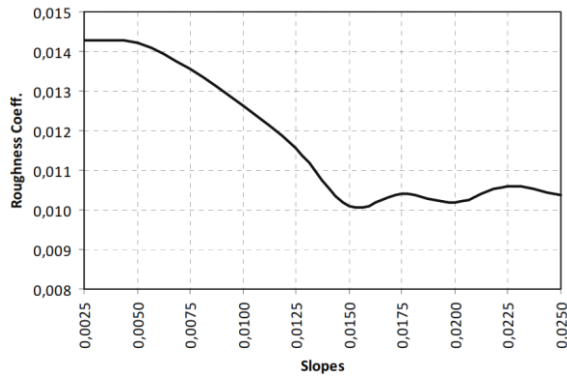


Figure 9. Graph of the relationship between the Manning roughness coefficient and variations in channel bottom slope for PVC lined material (25)

2. 3. Data Collection

The data collected were dependent variables data and independent variables data. Some of the dependent variable data include: a) the bottom width of the GFRP flume section (b_g) of 28.9 cm; b) the flume length (L_f) of 960 cm; c) the length of the flume lined with GFRP material (L_g) of 900 cm; d) GFRP flume height (T_g) of 31 cm; and e) the gravitational constant (g) is taken as 9.81 m/s². GFRP flume bottom slope data (S_g) was measured by adjusting the flume bottom slopes by increasing the flume elevation in the upstream section at 2 (two) cm intervals for 9 (nine) times to obtain nine different channel/flume bottom slope conditions. By dividing the difference in the height of the upstream and downstream of the flume by the length of the flume ($L_f = 960$ cm), the values of the nine-bottom slopes of the GFRP flume (S_g) are 0.0021; 0.0042; 0.0063; 0.0083; 0.0104; 0.0125; 0.0146; 0.0167; and 0.0188 respectively. Data collections of the independent variables in the GFRP flume were flow depth (h_g) and flow velocity (v_g). The flow depth in the GFRP flume (h_g) was obtained by directly measuring each water flow test's results with a point gauge. The average depth of water flow in the GFRP flume (h_r) is the flow depth used to measure the average flow velocity using a flow-meter device measured from the surface of the flow, where the h_r value is 0.6 h_g . The flow velocity in the GFRP flume (v_g) was measured directly using a flow-meter device.

2. 4. Data Processing and Analysis

After obtaining the hydraulic data of the water flow in the GFRP flume, then data processing was carried out to obtain the values of other flow parameters data in the flume, such as the wetted area (A_g); wetted perimeter (P_g), hydraulic radius (R_g); discharge that flow in the flume (Q_g); Manning roughness coefficient for GFRP materials (n_g); critical depth (h_{cg}); and flow velocity characteristics that occur using the Froude Number indicator. In the next stage, the calculation results obtained from the experimental test were compared with the results of testing with a mathematical model, i.e.,

HEC-RAS Software (26). If comparing the two models shows good results, it will proceed to the analysis and interpretation of the test data. However, if not, verifying, validating, and calibrating the data will be done first until the model performance shows appropriate results.

2. 5. Mathematical Equations

The inflow discharge through the GFRP flume (Q_f) was measured using the volumetric method. This method involved measuring the weight of water (W_w) flowing out of the downstream end of the GFRP flume using a bucket within a specific time interval (Δt). The volume of water (V_w) was then calculated by dividing the weight of water (W_w) by the specific gravity of water ($\gamma_w = 1$ g/cm³). There were three variations setting of pump discharge into the GFRP flume, i.e., low inflow discharge (Q_{f1}), medium inflow discharge (Q_{f2}), and high inflow discharge (Q_{f3}). The water flow setting for these three pump discharge variations was controlled by using two submersible pumps and adjusting valves in the pipeline network. For each of the three water storage experiments conducted in the bucket, the calculation for the pump discharge (Q_f) is determined using the following formula:

$$Q_f = \frac{1}{3} \sum_{i=1}^3 \frac{V_{wi}}{\Delta t_i} \quad (7)$$

Measurement of flow parameters in the GFRP flume (h_g and v_g) was conducted in the steady-state flow conditions, and the high-water level is parallel at several points in the middle of the flume segment. Other hydraulic parameters such as wetted area (A_g), wetted perimeter (P_g), and hydraulic radius (R_g) are calculated using the formula (25):

$$A_g = b_g h_g \quad (8)$$

$$P_g = b_g + 2h_g \quad (9)$$

$$R_g = \frac{A_g}{P_g} = \frac{b_g h_g}{b_g + 2h_g} \quad (10)$$

The discharge flowing in the GFRP flume (Q_g) is calculated using the following formula:

$$Q_g = v_g A_g \quad (11)$$

The value of the Manning roughness coefficient (n_g) obtained from the experimental test results is then determined using the following formula (22, 23):

$$n_g = \frac{1}{v_g} R_g^{2/3} S_g^{1/2} \quad (12)$$

Alternatively, it can also be calculated as follows:

$$n_g = \frac{R_g^{2/3} S_g^{1/2} A_g}{Q_g} \quad (13)$$

The critical depth occurring in the GFRP flume (h_{cg}) is calculated using the following equation (26):

$$h_{cg} = \sqrt[3]{\frac{Q_g^2}{b_g^2 g}} \tag{14}$$

If the critical depth (h_{cg}) is bigger than the measured flow depth (h_g), the flow is then at the super-critical state and otherwise is at the sub-critical state.

2. 6. Model Evaluation and Performance Assessment

According to Moriasi et al. (27), based on the recommendations of Legates and McCabe (28) and American Society of Civil Engineer (29) model evaluation involves using graphical techniques and quantitative statistics. The graphical techniques provide a visual assessment of model performance. Utilizing these essential techniques should typically be the first step in model evaluation. A familiar visual fit between observed and simulated constituent data indicates adequate calibration and validation within the simulated constituent range (27, 30). There are various quantitative statistical assessment methods (27), but this study will only use the Nash-Sutcliffe Efficiency (NSE) method. This method involves comparing the model simulation data with quantitative measurement data. The formula for calculating the NSE value is as follows (27, 31, 32):

$$NSE = 1 - \left[\frac{\sum_{i=1}^n (Y_i^{obs} - Y_i^{sim})^2}{\sum_{i=1}^n (Y_i^{obs} - Y^{mean})^2} \right] \tag{15}$$

where: n = the total number of observations; Y_i^{obs} = the i th observation for the constituent being evaluated; Y_i^{sim} = the i th simulated constituent value for the constituent being evaluated; Y^{mean} = the mean of observed data for the constituent being evaluated.

The best performance values from the predicted value or mathematical model with observational data or the physical model can be obtained if the NSE Index value = 1. A performance rating of the model results is carried out to assess performance in the model's verification and calibration process. The model performance is evaluated as "very good" if the NSE value exceeds 0.75. Model performance is evaluated as "good" if the NSE value ranges from 0.65 to equal/less than 0.75. The model performance is evaluated as "satisfactory" if the NSE value is 0.5 to equal/less than 0.65. The model performance is evaluated as "unsatisfactory" if the NSE value equals/less than 0.5. Table 1 summarizes the relationship between NSE Index and model performance ratings (27).

TABLE 1. Performance rating model with the NSE method

No.	Performance Rating	NSE Index
1.	Very good	0,75 < NSE ≤ 1,00
2.	Good	0,65 < NSE ≤ 0,75
3.	Satisfactory	0,5 < NSE ≤ 0,65
4.	Unsatisfactory	NSE ≤ 0,50

3. RESULTS AND DISCUSSION

3. 1. Calculation and Analysis of Pump Discharge Flowing into the GFRP Flume (Q_f) using the Volumetric Method

Calculation and validation of three variations of water pump discharge into the GFRP flume (Q_f), i.e., low inflow discharge (Q_{f1}), medium inflow discharge (Q_{f2}), and high inflow discharge (Q_{f3}) using the volumetric method are presented in Table 2.

From Table 2, data were calculated from three validated pump discharge variations that flow into the GFRP flume, such as low inflow discharge (Q_{f1}) of 7.83 l/s or 7,830 cm³/s; medium inflow discharge (Q_{f2}) of 11.60 l/s or 11,600 cm³/s; and high inflow discharge (Q_{f3}) of 14.88 l/s or 14,880 cm³/s.

3. 2. Calculation and Analysis of Water Flow Data on Physical Models

After the measurement and validation of the pump discharge have been completed, the flow depth (h_g) and flow velocity (v_g) that occurs in the flume were measured for each of the three discharge variations that flow into the flume (Q_{f1} , Q_{f2} , and Q_{f3}) and on nine variations of flume bottom slope (S_g). Using the GFRP flume width (b_g) of 28.9 cm, calculating the Manning roughness coefficient value (n_g), and analysis of other flow parameters are summarized and presented in Tables 3, 4 and 5, respectively.

From the physical modeling calculation result, the average Manning roughness coefficient (n_g) value for the three discharge variations (Q_f) is obtained: n_{g1} = 0.0083, n_{g2} = 0.0082, and n_{g3} = 0.0079. Calculations and data analysis will be carried out using a mathematical model to evaluate the reliability of the physical modeling results.

TABLE 2. Calculation and validation for low, medium, and high inflow discharge variations

No.	Inflow discharge type	Water Volume	Time Interval	Discharge	Average Discharge	
		V_w	Δt	Q_f	Q_f	Q_f
		l	s	l/s	l/s	cm ³ /s
1	Q_{f1} (Low Inflow Discharge)	28.05	3.64	7.72		
		32.38	4.02	8.05	7.83	7,830
		42.46	5.50	7.72		
2	Q_{f2} (Medium Inflow Discharge)	35.64	3.23	11.03		
		42.29	3.48	12.15	11.60	11,600
		42.97	3.70	11.61		
3	Q_{f3} (High Inflow Discharge)	40.32	2.69	14.99		
		38.27	2.56	14.95	14.88	14,880
		35.58	2.42	14.70		

TABLE 2. The results of the calculation of the physical model for water flow parameters at low inflow discharge conditions ($Q_{I1} = 7,830 \text{ cm}^3/\text{s}$)

No.	Channel Bottom Slopes	Flow Velocity	Flow Depth	Wetted Area	Wetted Perimeter	Hydraulic Radius	Flow Discharge	Manning Roughness Coefficient	Critical Depth	Characteristic of Flow Velocity
	S_g	v_g	h_g	A_g	P_g	R_g	Q_g	n_{g1}	h_{cg}	h_{cg}/h_g
	(cm/cm)	(cm/s)	(cm)	(cm ²)	(cm)	(cm)	(cm ³ /s)	-	(cm)	
1	0.0021	50.8	5.20	150.28	39.30	3.82	7,634	0.0102	4.14	subcritical
2	0.0042	65.0	3.67	106.06	36.24	2.93	6,897	0.0094	3.87	supercritical
3	0.0063	83.3	3.00	86.70	34.90	2.48	7,223	0.0081	3.99	supercritical
4	0.0083	91.4	2.72	78.61	34.34	2.29	7,188	0.0080	3.98	supercritical
5	0.0104	102.6	2.70	78.03	34.30	2.27	8,007	0.0080	4.28	supercritical
6	0.0125	113.8	2.52	72.83	33.94	2.15	8,287	0.0076	4.38	supercritical
7	0.0146	116.8	2.46	71.09	33.82	2.10	8,307	0.0079	4.38	supercritical
8	0.0167	120.9	2.42	69.94	33.74	2.07	8,456	0.0081	4.44	supercritical
9	0.0188	125.0	2.20	63.58	33.30	1.91	7,945	0.0078	4.26	supercritical
Average of Manning Roughness Coefficient (n_{g1}) =								0.0083		

TABLE 3. The results of the calculation of the physical model for water flow parameters at medium inflow discharge conditions ($Q_{I2} = 11,600 \text{ cm}^3/\text{s}$)

No.	Channel Bottom Slopes	Flow Velocity	Flow Depth	Wetted Area	Wetted Perimeter	Hydraulic Radius	Flow Discharge	Manning Roughness Coefficient	Critical Depth	Characteristic of Flow Velocity
	S_g	v_g	h_g	A_g	P_g	R_g	Q_g	n_{g2}	h_{cg}	h_{cg}/h_g
	(cm/cm)	(cm/s)	(cm)	(cm ²)	(cm)	(cm)	(cm ³ /s)	-	(cm)	
1	0.0021	62.0	5.77	166.75	40.44	4.12	10,335	0.0088	5.07	subcritical
2	0.0042	85.3	4.70	135.83	38.30	3.55	11,592	0.0082	5.47	supercritical
3	0.0063	100.6	4.07	117.62	37.04	3.18	11,831	0.0079	5.55	supercritical
4	0.0083	112.8	3.70	106.93	36.30	2.95	12,059	0.0077	5.62	supercritical
5	0.0104	117.9	3.58	103.32	36.05	2.87	12,177	0.0081	5.66	supercritical
6	0.0125	121.9	3.40	98.26	35.70	2.75	11,980	0.0084	5.60	supercritical
7	0.0146	128.0	3.19	92.19	35.28	2.61	11,802	0.0083	5.54	supercritical
8	0.0167	133.1	3.03	87.57	34.96	2.50	11,655	0.0083	5.49	supercritical
9	0.0188	138.2	2.92	84.39	34.74	2.43	11,660	0.0083	5.50	supercritical
Average of Manning Roughness Coefficient (n_{g2}) =								0.0082		

TABLE 5. The results of the calculation of the physical model for water flow parameters at high inflow discharge conditions ($Q_{I3} = 14,880 \text{ cm}^3/\text{s}$)

No.	Channel Bottom Slopes	Flow Velocity	Flow Depth	Wetted Area	Wetted Perimeter	Hydraulic Radius	Flow Discharge	Manning Roughness Coefficient	Critical Depth	Characteristic of Flow Velocity
	S_g	v_g	h_g	A_g	P_g	R_g	Q_g	n_{g3}	h_{cg}	h_{cg}/h_g
	(cm/cm)	(cm/s)	(cm)	(cm ²)	(cm)	(cm)	(cm ³ /s)	-	(cm)	
1	0.0021	66.0	6.41	185.25	41.72	4.44	12,234	0.0087	5.67	subcritical
2	0.0042	101.6	5.07	146.52	39.04	3.75	14,887	0.0071	6.47	supercritical
3	0.0063	114.8	4.62	133.52	38.14	3.50	15,329	0.0074	6.59	supercritical
4	0.0083	122.9	4.27	123.40	37.44	3.30	15,171	0.0076	6.55	supercritical

5	0.0104	130.0	4.18	120.66	37.25	3.24	15,691	0.0080	6.70	supercritical
6	0.0125	136.1	3.92	113.29	36.74	3.08	15,423	0.0081	6.62	supercritical
7	0.0146	142.2	3.58	103.32	36.05	2.87	14,696	0.0080	6.41	supercritical
8	0.0167	147.3	3.52	101.66	35.94	2.83	14,976	0.0081	6.49	supercritical
9	0.0188	153.4	3.32	95.95	35.54	2.70	14,720	0.0080	6.42	supercritical
Average of Manning Roughness Coefficient (n_{g3}) =								0.0079		

3. 3. Initial Simulation of Water Flow with Mathematical Models

Initial simulation for calculating and analyzing water flow data with mathematical models will be applied using HEC-RAS software. In the physical model, several water flow parameters (such as flow depth (h_g), flow velocity (v_g), and inflow discharge (Q_f)) are measured/calculated first and then inputted as data variables in a mathematical equation to calculate other water flow parameters, including the value of the Manning roughness coefficient (n_g). In the mathematical model (using the HEC-RAS application), some of the dependent variable data used in the physical model are also used as input data for model simulation, like the bottom width of the GFRP flume (b_g), the height of the GFRP flume (T_g), the nine variations of channel bottom slope (S_g), and the three variations of inflow discharge (Q_f). In addition, data on the Manning roughness coefficient value (n_g) obtained from the results of physical modeling were also used as input data in the initial simulation of the HEC-RAS model. After running the model under steady-state flow conditions, the output data from this model simulation process are flow depth (h_s), wetted area (A_s), wetted

perimeter (P_s), hydraulic radius (R_s), flow velocity (v_s), and critical depth (h_{cs}). Initial simulation results for calculating water flow parameters using the HEC-RAS software for each of the three discharge variations (Q_{f1} , Q_{f2} , and Q_{f3}) are then summarized and presented in Tables 6, 7 and 8, respectively.

3. 4. Comparison and Assessment of Physical Model Performance with Initial Simulation of Mathematical Models

The results of calculating the flow depth (h_s) resulting from the initial simulation of the mathematical model (HEC-RAS) are then compared with the results of calculating the flow depth (h_g) resulting from physical modeling. The comparison of h_s and h_g values for three variations of flow discharge (Q_{f1} , Q_{f2} , and Q_{f3}) and nine variations of channel bottom slope (S_g) is then displayed in a graphic presented in Figure 10. From the graphic in Figure 10. it can be seen that although the flow depth profile (h_g) in the physical model and flow depth profile (h_s) in the mathematical model have similar curves, at several locations of the channel bottom slope (S_g), there are significant deviations and anomaly conditions of the flow depth values (h_g and h_s).

TABLE 4. Calculation results from initial mathematical model simulation (HEC-RAS) for water flow parameters at low inflow discharge conditions ($Q_{f1} = 7,830 \text{ cm}^3/\text{s}$)

No.	Channel Bottom Slopes	Manning Roughness Coefficient	Flow Velocity	Flow Depth	Flow Discharge	Wetted Area	Wetted Perimeter	Hydraulic Radius	Critical Depth	Characteristic of Flow Velocity
	S_s (cm/cm)	n_s -	v_s (cm/s)	h_s (cm)	Q_s (cm^3/s)	A_s (cm^2)	P_s (cm)	R_s (cm)	h_{cs} (cm)	h_{cs}/h_s
1	0.0021	0.0102	53.99	5.02	7,830	145.08	38.94	3.73	4.21	subcritical
2	0.0042	0.0094	71.34	3.79	7,830	109.53	36.48	3.00	4.21	supercritical
3	0.0063	0.0081	74.60	3.63	7,830	104.91	36.16	2.90	4.21	supercritical
4	0.0083	0.0080	90.92	2.98	7,830	86.12	34.86	2.47	4.21	supercritical
5	0.0104	0.0080	95.32	2.84	7,830	82.08	34.58	2.37	4.21	supercritical
6	0.0125	0.0076	105.54	2.57	7,830	74.27	34.04	2.18	4.21	supercritical
7	0.0146	0.0079	98.53	2.75	7,830	79.48	34.40	2.31	4.21	supercritical
8	0.0167	0.0081	118.69	2.28	7,830	65.89	33.46	1.97	4.21	supercritical
9	0.0188	0.0078	124.36	2.18	7,830	63.00	33.26	1.89	4.21	supercritical
Average of Manning Roughness Coefficient from Numeric Simulation (n_{s1}) =								0.0083		

TABLE 7. Calculation results from the initial mathematical model simulation (HEC-RAS) for water flow parameters at medium inflow discharge conditions ($Q_2 = 11,600 \text{ cm}^3/\text{s}$)

No.	Channel Bottom Slopes	Manning Roughness Coefficient	Flow Velocity	Flow Depth	Flow Discharge	Wetted Area	Wetted Perimeter	Hydraulic Radius	Critical Depth	Characteristic of Flow Velocity
	S_s	n_s	v_s	h_s	Q_s	A_s	P_s	R_s	h_{cs}	h_{cs}/h_s
	(cm/cm)	-	(cm/s)	(cm)	(cm^3/s)	(cm^2)	(cm)	(cm)	(cm)	
1	0.0021	0.0088	67.03	5.99	11,600	173.11	40.88	4.23	5.48	subcritical
2	0.0042	0.0082	76.25	5.26	11,600	152.01	39.42	3.86	5.48	supercritical
3	0.0063	0.0079	101.18	3.97	11,600	114.73	36.84	3.11	5.48	supercritical
4	0.0083	0.0077	107.01	3.75	11,600	108.38	36.40	2.98	5.48	supercritical
5	0.0104	0.0081	111.49	3.6	11,600	104.04	36.10	2.88	5.48	supercritical
6	0.0125	0.0084	123.55	3.25	11,600	93.93	35.40	2.65	5.48	supercritical
7	0.0146	0.0083	126.75	3.17	11,600	91.61	35.24	2.60	5.48	supercritical
8	0.0167	0.0083	109.21	3.67	11,600	106.06	36.24	2.93	5.48	supercritical
9	0.0188	0.0083	133.88	2.99	11,600	86.41	34.88	2.48	5.48	supercritical
Average of Manning Roughness Coefficient from Numeric Simulation (n_{s2}) =									0.0082	

TABLE 8. Calculation results from the initial mathematical model simulation (HEC-RAS) for water flow parameters at high inflow discharge conditions ($Q_3 = 14,880 \text{ cm}^3/\text{s}$)

No.	Channel Bottom Slopes	Manning Roughness Coefficient	Flow Velocity	Flow Depth	Flow Discharge	Wetted Area	Wetted Perimeter	Hydraulic Radius	Critical Depth	Characteristic of Flow Velocity
	S_s	n_s	v_s	h_s	Q_s	A_s	P_s	R_s	h_{cs}	h_{cs}/h_s
	(cm/cm)	-	(cm/s)	(cm)	(cm^3/s)	(cm^2)	(cm)	(cm)	(cm)	
1	0.0021	0.0087	73.61	7.00	14,880	202.30	42.90	4.72	6.47	subcritical
2	0.0042	0.0071	91.98	5.60	14,880	161.84	40.10	4.04	6.47	supercritical
3	0.0063	0.0074	112.47	4.58	14,880	132.36	38.06	3.48	6.47	supercritical
4	0.0083	0.0076	121.88	4.23	14,880	122.25	37.36	3.27	6.47	supercritical
5	0.0104	0.0080	126.77	4.06	14,880	117.33	37.02	3.17	6.47	supercritical
6	0.0125	0.0081	136.08	3.78	14,880	109.24	36.46	3.00	6.47	supercritical
7	0.0146	0.0080	143.27	3.60	14,880	104.04	36.10	2.88	6.47	supercritical
8	0.0167	0.0081	145.32	3.54	14,880	102.31	35.98	2.84	6.47	supercritical
9	0.0188	0.0080	153.89	3.34	14,880	96.53	35.58	2.71	6.47	Supercritical
Average of Manning Roughness Coefficient from Numeric Simulation (n_{s3}) =									0.0079	

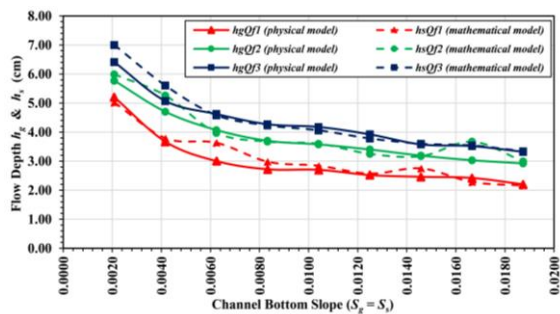


Figure 10. Graphic comparison between the flow depth (h_s) in the initial simulation of the mathematical model (HEC-RAS) and the flow depth (h_g) in the physical model for three variations of inflow discharge (Q_f)

Furthermore, the results of the calculation of flow velocity (v_s) resulting from the initial simulation of the mathematical model (HEC-RAS) are also compared with the results of calculating the flow velocity (v_g) resulting from physical model. Comparison of v_s and v_g values for the three variations of flow discharge (Q_{f1} , Q_{f2} , and Q_{f3}) and the nine variations of channel bottom slope (S_g) are then displayed in the graphic presented in Figure 11.

From the graphic in Figure 11, it can be seen that although the flow velocity profile (v_g) in the physical model and the flow velocity profile (v_s) in the initial simulation of the mathematical model have similar curves at several locations of the channel bottom slope (S_g), there are significant deviations and anomaly

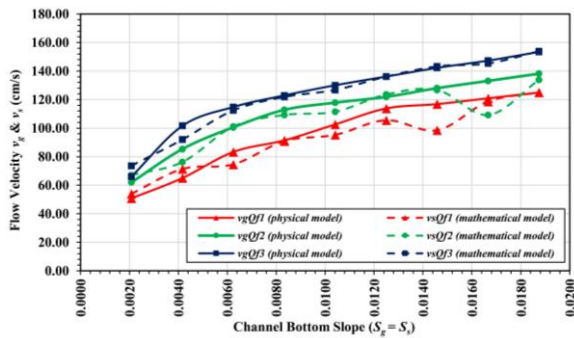


Figure 11. Graphic comparison between flow velocity (v_s) in the initial simulation of the mathematical model (HEC-RAS) and flow velocity (v_g) in the physical model for three variations of inflow discharge (Q_f)

conditions in the flow velocity values (v_g and v_s). A quantitative accuracy assessment evaluates the performance of the physical model by using the Nash-Sutcliffe Efficiency (NSE) model. The assessment calculates and compares the NSE values for the flow depth (h) and flow velocity (v) parameters between the physical model and the initial simulation of the mathematical model. The resulting NSE values are then presented in Table 9. Based on the values in Table 9, the NSE index for flow depth (h) and flow velocity (v) exceeds 0.75. Consequently, the overall performance of the model, considering three variations of inflow discharge (Q_f), can be stated as “very good”.

Even though the NSE indexes already have a “very good” performance rating, in order to provide better

TABLE 9. Recapitulation of the results of the Quantitative Accuracy Assessment (NSE) between the observed data and the initial simulation results of the mathematical model

No.	Flow Discharge Type	NSE Index for flow depth	Performance Rating	NSE Index for flow velocity	Performance Rating
		NSE (h_g)		NSE (v_g)	
1	Q_{f1} (low inflow discharge)	0.908	very good	0.892	very good
2	Q_{f2} (medium inflow discharge)	0.881	very good	0.844	very good
3	Q_{f3} (high inflow discharge)	0.910	very good	0.971	very good

modeling accuracy, the calibration process will still be carried out, especially for some conditions of channel bottom slope (S_g) where the flow parameters (flow depth and velocity) provide anomaly condition and different deviation values-quite significant.

Model calibrations are carried out for low inflow discharge conditions ($Q_{f1} = 7,830 \text{ cm}^3/\text{s}$) and medium inflow discharge conditions ($Q_{f2} = 11,600 \text{ cm}^3/\text{s}$) because, apart from having an anomaly and a significant deviation value, the NSE indexes for flow depth and flow velocity are still below 0.9. For conditions of high inflow discharge ($Q_{f3} = 14,880 \text{ cm}^3/\text{s}$), the calibration process is not carried out because the NSE indexes for flow depth and velocity respectively are already reached an exceptionally high value of 0.910 and 0.971 (≈ 1).

3. 5. Model Evaluation and Performance Assessment

The calibration process involves modifying the input data of the initial Manning roughness coefficient (n_g) value in the HEC-RAS simulation to reduce further the deviation profiles and anomaly conditions are shown in Figures 10 and 11 and achieve smooth graphic curves. For low inflow discharge conditions ($Q_{f1} = 7,830 \text{ cm}^3/\text{s}$), the results of calibration are the Manning roughness coefficient values for two-channel bottom slopes (S_g) that exhibit relatively high flow depth deviation values (h_g and h_s), specifically S_{g3} and S_{g7} .

For the channel bottom slope of the S_{g3} , the initial n_g value of 0.0081 is calibrated to $n_s = 0.0080$. Similarly, for

the channel bottom slope of the S_{g7} , the initial n_g value of 0.0078 is calibrated to $n_s = 0.0077$. Once the calibration process for the Manning roughness coefficient value is completed, the HEC-RAS model will be running again and summarize the calculation results obtained from the model simulation. These results are then presented in Table 10.

For medium inflow discharge conditions ($Q_{f2} = 11,600 \text{ cm}^3/\text{s}$), the Manning coefficient values were calibrated on two channel bottom slopes (S_g), which had relatively high flow depth deviation values (h_g and h_s), namely S_{g2} and S_{g8} . For the channel bottom slope of the S_{g2} , the initial n_g value is 0.0082 and calibrated to $n_s = 0.0080$. For the channel bottom slope of the S_{g8} , the initial n_g value is 0.0083 and calibrated to $n_s = 0.0081$. After the calibration process for the Manning roughness coefficient value is carried out, the HEC-RAS model is running again, and the calculation results from the model simulation are summarized and presented in Table 11.

The calibration process was not carried out for high inflow discharge conditions ($Q_{f3} = 14,880 \text{ cm}^3/\text{s}$), so the initial simulation results of the mathematical models in Table 8 will still be used for further data analysis and interpretation. After the calibration process of the Manning roughness coefficient value is carried out, the results of the calculation of the flow parameters resulting from the mathematical modeling are then compared again with the results of the estimation of the flow parameters resulting from the physical modeling.

TABLE 5. Calculation results from the next mathematical model simulation (HEC-RAS) for water flow parameters at low inflow discharge conditions ($Q_{f1} = 7,830 \text{ cm}^3/\text{s}$)

No.	Channel Bottom Slopes	Manning Roughness Coefficient	Flow Velocity	Flow Depth	Flow Discharge	Wetted Area	Wetted Perimeter	Hydraulic Radius	Critical Depth	Characteristic of Flow Velocity
	S_s	n_{s1}	v_s	h_s	Q_s	A_s	P_s	R_s	h_{cs}	h_{cs}/h_s
	(cm/cm)	-	(cm/s)	(cm)	(cm ³ /s)	(cm ²)	(cm)	(cm)	(cm)	
1	0.0021	0.0102	53.99	5.02	7,830	145.08	38.94	3.73	4.21	subcritical
2	0.0042	0.0094	71.34	3.79	7,830	109.53	36.48	3.00	4.21	supercritical
3	0.0063	0.0080	89.86	3.02	7,830	87.28	34.94	2.50	4.21	supercritical
4	0.0083	0.0080	90.92	2.98	7,830	86.12	34.86	2.47	4.21	supercritical
5	0.0104	0.0080	95.32	2.84	7,830	82.08	34.58	2.37	4.21	supercritical
6	0.0125	0.0076	105.54	2.57	7,830	74.27	34.04	2.18	4.21	supercritical
7	0.0146	0.0077	110.33	2.46	7,830	71.09	33.82	2.10	4.21	supercritical
8	0.0167	0.0081	118.69	2.28	7,830	65.89	33.46	1.97	4.21	supercritical
9	0.0188	0.0078	124.36	2.18	7,830	63.00	33.26	1.89	4.21	supercritical
Average of Manning Roughness Coefficient from Numeric Simulation (n_{s1}) =									0.0083	

TABLE 11. Calculation results from next mathematical model simulation (HEC-RAS) for water flow parameters at medium inflow discharge conditions ($Q_{f2} = 11,600 \text{ cm}^3/\text{s}$)

No.	Channel Bottom Slopes	Manning Roughness Coefficient	Flow Velocity	Flow Depth	Flow Discharge	Wetted Area	Wetted Perimeter	Hydraulic Radius	Critical Depth	Characteristic of Flow Velocity
	S_s	n_{s2}	v_s	h_s	Q_s	A_s	P_s	R_s	h_{cs}	h_{cs}/h_s
	(cm/cm)	-	(cm/s)	(cm)	(cm ³ /s)	(cm ²)	(cm)	(cm)	(cm)	
1	0.0021	0.0088	67.03	5.99	11,600	173.11	40.88	4.23	5.48	subcritical
2	0.0042	0.0080	77.34	5.19	11,600	149.99	39.28	3.82	5.48	supercritical
3	0.0063	0.0079	101.18	3.97	11,600	114.73	36.84	3.11	5.48	supercritical
4	0.0083	0.0077	107.01	3.75	11,600	108.38	36.40	2.98	5.48	supercritical
5	0.0104	0.0081	111.49	3.6	11,600	104.04	36.10	2.88	5.48	supercritical
6	0.0125	0.0084	123.55	3.25	11,600	93.93	35.40	2.65	5.48	supercritical
7	0.0146	0.0083	126.75	3.17	11,600	91.61	35.24	2.60	5.48	supercritical
8	0.0167	0.0081	133.88	2.99	11,600	86.41	34.88	2.48	5.48	supercritical
9	0.0188	0.0083	133.88	2.99	11,600	86.41	34.88	2.48	5.48	supercritical
Average of Manning Roughness Coefficient from Numeric Simulation (n_{s2}) =									0.0082	

Comparison of the flow depth value (h_s) resulting from mathematical modeling with the flow depth value (h_g) resulting from physical modeling for three variations of flow discharge (Q_{f1} , Q_{f2} , and Q_{f3}) is then displayed again in the graphic as presented in Figure 12.

From the graphic in Figure 12, it can be seen that the flow depth profile (h_g) in the physical model and flow depth profile (h_s) in the mathematical model still have similar curves, and the deviations that occur at several locations of the channel bottom slope (S_g) have also decreased.

Furthermore, the comparison of flow velocity values (v_s) resulting from mathematical modeling with flow velocity values (v_g) resulting from physical modeling for three variations of flow discharge (Q_{f1} , Q_{f2} , and Q_{f3}) are displayed again in the graphic as presented in Figure 13. From the graphic in Figure 13, it can be seen that the flow velocity profiles (v_g) in the physical model and the flow velocity profiles (v_s) in the mathematical model still have similar curves, and the deviations that occur at several locations of the channel bottom slope (S_g) have also decreased.

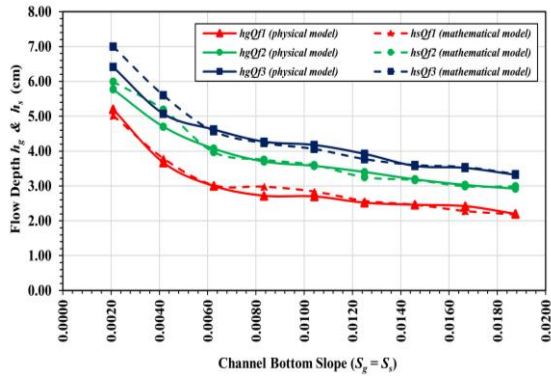


Figure 12. Comparison graphic between flow depth (h_s) in the mathematical model and flow depth (h_g) in the physical model for three variations of inflow discharge (Q_f) after the calibration process

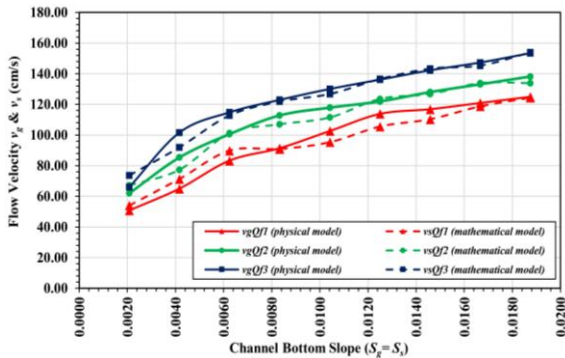


Figure 13. Graphic comparison between flow velocity (v_s) in the mathematical model and flow velocity (v_g) in the physical model for three variations of inflow discharge (Q_f) after the calibration process

Finally, the comparison of the calibration value of the Manning roughness coefficient (n_s) resulting from mathematical modeling with the value of the Manning roughness coefficient (n_g) resulting from physical modeling for three variations of flow discharge (Q_{f1} , Q_{f2} , and Q_{f3}) is displayed in the graphic as presented in Figure 14.

The graphic in Figure 14 shows that the profile of the Manning roughness coefficient (n_g) in the physical model and the profile of the Manning roughness coefficient (n_s) in the mathematical model have similar curves. The deviations at several locations of the channel bottom slope (S_g) are also relatively small. After the mathematical model calibration process has been completed, a reassessment of the overall model performance (both the calibration process and the non-calibration process) is carried out using the Nash-Sutcliffe Efficiency (NSE) method.

The results of the calculation of the NSE values for the parameters of flow depth (h_g), flow velocity (v_g), and Manning roughness coefficient (n_g) for three variations

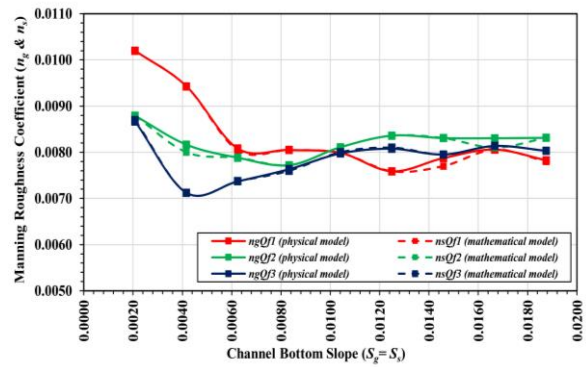


Figure 14. Graphic comparison between the Manning roughness coefficient (n_s) in the mathematical model and the Manning roughness coefficient (n_g) in the physical model for three variations of inflow discharge (Q_f) after the calibration process

of inflow discharge (Q_{f1} , Q_{f2} , and Q_{f3}) are then presented again in Table 12. Table 12 shows that the NSE Index values for the three flow parameters (h_g , v_g , and n_g) are better when compared to the NSE Index values before calibration (see Table 9 again).

3. 6. Flow Characteristic and Manning Roughness Coefficient

The final discussion of the flow characteristics and the value of the Manning roughness coefficient is carried out by taking data from the physical model testing, i.e., data in Tables 3, 4 and 5 as well as graphical analysis in Figures 12, 13 and 14. Based on the graphic presented in Figure 12, it can be interpreted that with increasing discharge (Q_{f1} to Q_{f3}), the flow depth (h) will also increase. However, as the bottom slope (S) increases, the flow depth (h) will decrease.

Based on the graphic presented in Figure 13, it can be interpreted that the flow velocity (v) will increase with increasing discharge (Q_{f1} to Q_{f3}) and also the bottom slope of the channel (S). Based on the data presented in Table 3 (for Q_{f1}), Table 4 (for Q_{f2}), and Table 5 (for Q_{f3}), and regarding the Froude Number indicator, in this modeling, two characteristics of water flow are formed, namely subcritical flow and supercritical flow. Subcritical flow occurs in three conditions of inflow discharge (Q_f) but only on the flume's first bottom slope (S_{g1}). These results show that in these flow conditions, the effect of inertial forces is still greater than gravitational forces. From the second channel bottom slope (S_{g2}) to the ninth channel bottom slope (S_{g9}), the flow characteristics change to supercritical flow for the three inflow discharge conditions (Q_f). These results show that the effect of gravitational forces is more significant in these flow conditions than inertial forces.

Based on the graphic presented in Figure 14, it can be interpreted that the value of the Manning roughness coefficient (n) tends to change (not stable) if the inflow discharge (Q) or channel bottom slope (S) is changed.

ABLE 6. Recapitulation of the results of the quantitative accuracy assessment (Nash-Sutcliffe Efficiency method) after the calibration process with the mathematical model

No.	Flow Discharge Type	NSE Index for flow depth		NSE Index for flow velocity		NSE Index for Manning Roughness Coefficient	
		NSE (h_g)	PR	NSE (v_g)	PR	NSE (n_g)	PR
1	Q_{f1} (low inflow discharge)	0.977	Very good	0.952	Very good	0.995	Very good
2	Q_{f2} (medium inflow discharge)	0.951	Very good	0.960	Very good	0.908	Very good
3	Q_{f3} (high inflow discharge)	0.910	Very good	0.971	Very good	0.999	Very good

(*) PR = Performance Rating

The value of the Manning roughness coefficient (n) tends to be high when the bottom slope of the channel (S) is mild. However, starting from the third bottom slope ($S_{g3} = 0.0063$), the value of the Manning roughness coefficient (n) tends to be more stable. However, some values of the Manning roughness coefficient (n) still tend to increase or decrease, but the value of the deviation that occurs is relatively minor. The stability of the Manning roughness coefficient (n) value occurs in supercritical flow conditions.

Based on Tables 3 and 10, for low inflow discharge ($Q_{f1} = 7,830 \text{ cm}^3/\text{s}$), the value of the Manning roughness coefficient (n) is in the range of 0.0076 to 0.0102, while the average value is 0.0083. Based on Tables 4 and 11, for medium inflow discharge ($Q_{f2} = 11,600 \text{ cm}^3/\text{s}$), the value of the Manning roughness coefficient (n) is in the range of 0.0077 to 0.0088, while the average value is 0.0082. Based on Tables 5 and 8, for high inflow discharge ($Q_{f3} = 14,880 \text{ cm}^3/\text{s}$), the value of the Manning roughness coefficient (n) is in the range of 0.0071 to 0.0087, while the average value is 0.0079. Overall, for the three variations of inflow discharge (Q_{f1} , Q_{f2} , and Q_{f3}) and nine variations of channel bottom slope (S_{g1} to S_{g9}), the value of the Manning roughness coefficient (n) is in the range of 0.0071 to 0.0102, while the average value is 0.0081.

3. 7. Verification the Accuracy of the Proposed Method

Two verification methods will be carried out to analyze the accuracy of this proposed research method and the Manning roughness coefficient value obtained from the research results. The first verification was carried out by comparing the results of this research with those conducted by Mera and Robi [28]. To test the accuracy of the proposed method carried out in this research, several graphic analyses of the results of this research will be compared with graphic analyses of the results of research carried out by Mera and Robi [28], which are as follows:

1. For the relationship between flow depth (h) and channel bottom slope (S), for each of the three variations of flow discharge (Q_{f1} , Q_{f2} , and Q_{f3}), the

graphic profile obtained from the results of this experimental test (Figure 12) is similar to the graphic profile obtained from the results of previous research conducted by Mera and Robi [28] (Figure 8).

2. For the relationship between the Manning roughness coefficient (n) and the channel bottom slope (S), for each of the three variations in flow discharge (Q_{f1} , Q_{f2} , and Q_{f3}), the graphic profile obtained from the results of this experimental test (Figure 14) has similarity to the graphic profile obtained from the previous research results of Mera and Robi (24) (Figure 9).

The second verification was carried out by comparing the Manning roughness coefficient (n) value for GFRP material obtained from this research with the n value of GFRP material from commercial piping products Grandpipe®¹ and Jiubo Composite®² and the n value for flexible GFRP material obtained from the results of research conducted by Okazawa et al. (21). The Manning roughness coefficient values (n) for the three GFRP material products range from 0.0084 to 0.0094. The value of the Manning roughness coefficient (n) for GFRP material obtained from the results of this study ($n = 0.0081$) is slightly smaller than the range of the three n values.

3. 8. The Performance Comparison Between Improved and Traditional Material

A comparative hydraulic analysis will be carried out between the flow depth in the GFRP material ($n = 0.0081$) from experimental test results in the laboratory and the flow depth in the concrete material ($n = 0.0143$) and stone masonry material ($n = 0.0167$) (1) from the results of analytical calculations using the Manning equation. Analysis of flow depth data for the three types of material was carried out using three variations of inflow discharge (Q_f) and nine variations of channel bottom slope (S_g), where the results of calculations and data processing are presented in Table 13.

The results of processing the flow depth data in Table 13 are then processed further in graphical form, as presented in Figure 15.

¹ <https://grandpipe.com/en/product-information>

² <https://www.aldfpr.com/News/Comparison-of-FRP-Pipe-and-pipe-flow-185.html>

TABLE 7. Comparison of flow depth (h) in the channel for conditions of three variations inflow discharge (Q_f) and nine variations of channel bottom slope (S_g) among GFRP material, concrete material, and stone masonry material

No.	Channel bottom slope S_g	Low Inflow Discharge (Q_{f1})			Medium Inflow Discharge (Q_{f2})			High Inflow Discharge (Q_{f3})		
		Flow Depth (GFRP)	Flow Depth (Concrete)	Flow Depth (Stone Masonry)	Flow Depth (GFRP)	Flow Depth (Concrete)	Flow Depth (Stone Masonry)	Flow Depth (GFRP)	Flow Depth (Concrete)	Flow Depth (Stone Masonry)
		h_g	h_c	h_{sm}	h_g	h_c	h_{sm}	h_g	h_c	h_{sm}
	(cm/cm)	(cm)	(cm)	(cm)	(cm)	(cm)	(cm)	(cm)	(cm)	(cm)
1	0.0021	5.2	6.65	7.41	5.77	8.75	9.77	6.41	10.45	11.7
2	0.0042	3.67	5.26	5.84	4.7	6.87	7.65	5.07	8.17	9.11
3	0.0063	3	4.59	5.09	4.07	5.98	6.65	4.62	7.09	7.9
4	0.0083	2.72	4.18	4.63	3.7	5.43	6.03	4.27	6.43	7.15
5	0.0104	2.7	3.88	4.3	3.58	5.03	5.59	4.18	5.95	6.62
6	0.0125	2.52	3.66	4.05	3.4	4.74	5.26	3.92	5.6	6.22
7	0.0146	2.46	3.48	3.85	3.19	4.5	4.99	3.58	5.31	5.9
8	0.0167	2.42	3.33	3.68	3.03	4.31	4.77	3.52	5.08	5.64
9	0.0188	2.2	3.2	3.54	2.92	4.14	4.59	3.32	4.89	5.42
Average Flow Depth (cm)		2.99	4.25	4.71	3.82	5.53	6.14	4.32	6.55	7.30
Flow depth comparison of h_g to h_c and h_{sm} (%)			70.35	63.48		69.08	62.21		65.95	59.18
Efficiency of using GFRP materials compared to concrete and stone masonry (%)			29.65	36.52		30.92	37.79		34.05	40.82

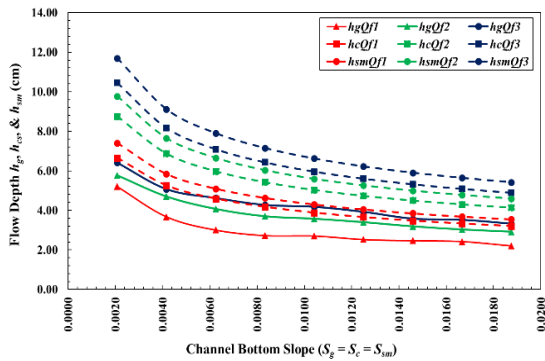


Figure 15. Comparison of flow depth (h) for conditions of three variations of inflow discharge (Q_f) and nine variations of channel bottom slope (S_g) among GFRP, concrete, and stone masonry materials

From the results of the data analysis in Table 13 and Figure 15, it can be seen that for conditions with three variations of inflow discharge (Q_f) and nine variations of channel bottom slope (S_g), as well as a fixed channel/flume bottom width ($b_g = 28.9$ cm), then the flow depth for GFRP material (h_g) is lower than the flow depth for concrete material (h_c) and the flow depth for stone masonry material (h_{sm}).

By taking the average flow depth value, for low inflow discharge conditions (Q_{f1}), the average flow depth value for GFRP material is $h_g = 2.99$ cm; the average flow

depth value for concrete material is $h_c = 4.25$ cm; and the average flow depth value for stone masonry material is $h_{sm} = 4.71$ cm (Figure 16). For medium inflow discharge conditions (Q_{f2}), the average flow depth value for GFRP material is $h_g = 3.82$ cm; the average flow depth value for concrete material is $h_c = 5.53$ cm; and the average flow depth value for stone masonry material is $h_{sm} = 6.14$ cm (Figure 17). For high inflow discharge conditions (Q_{f3}), the average flow depth value for GFRP material is $h_g = 4.32$ cm; the average flow depth value for concrete material is $h_c = 6.55$ cm; and the average flow depth value for stone masonry material is $h_{sm} = 7.30$ cm (Figure 18).

From the results of the data analysis, for the same values of discharge (Q_g), channel bottom width (b_g), and channel bottom slope (S_g), the flow depth for GFRP material (h_g) is lower than the flow depth for lined concrete material (h_c) and stone masonry material (h_{sm}) or can be written in the form: $h_g < h_c < h_{sm}$. Furthermore, for the condition that the bottom width of the cross-section is the same, the wet cross-sectional area of the GFRP material (A_g) is smaller than the wet cross-sectional area of the concrete material (A_c) as well as the wet cross-sectional area of the stone masonry material (A_{sm}), or can be written in the form $A_g < A_c < A_{sm}$.

When assessing the outcomes of a performance analysis of channel materials involving GFRP (Glass Fiber Reinforced Polymer) compared to traditional materials such as concrete and stone masonry, it is imperative to evaluate the effectiveness of GFRP's

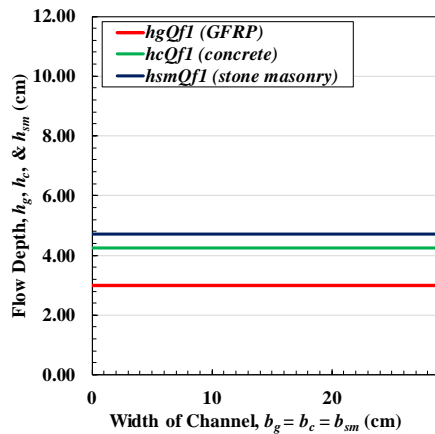


Figure 16. Comparison of average flow depth (h) for low inflow discharge (Q_1) among GFRP, concrete, and stone masonry lined material

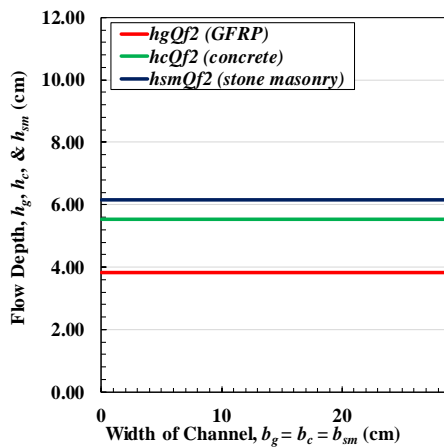


Figure 17. Comparison of average flow depth (h) for medium inflow discharge (Q_2) among GFRP, concrete, and stone masonry lined material

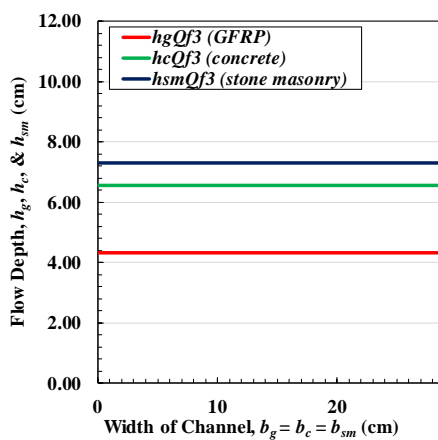


Figure 18. Comparison of average flow depth (h) for high inflow discharge (Q_3) among GFRP, concrete, and stone masonry lined material

performance. This evaluation of performance efficiency primarily focuses on the hydraulic aspect, explicitly comparing the flow depth within GFRP channel linings to that within concrete and stone masonry channel linings. The flow efficiency in a channel is significantly influenced by the Manning coefficient, which characterizes the smoothness or roughness of the channel's surface. In this particular scenario, GFRP exhibits a lower Manning coefficient (0.0081) in contrast to concrete (0.0143) and stone masonry (0.0167), indicating greater efficiency than traditional materials. Based on Table 13, Figure 19 presents a visual representation of the performance efficiency comparison between using GFRP channels and using concrete and stone masonry traditional channels.

Based on the results of this analysis, as shown in Table 13 and Figure 19, it can be concluded that at low inflow discharge, the flow depths in channels with GFRP lining are 29.65% more efficient than in channels with concrete lining and 36.52% more efficient than in channels with stone masonry lining. At medium inflow discharge, the flow depths in channels with GFRP lining are 30.92% more efficient than in channels with concrete lining and 37.79% more efficient than in channels with stone masonry lining. At high inflow discharge, the flow depths in channels with GFRP lining are 34.05% more efficient than in channels with concrete lining and 40.82% more efficient than in channels with stone masonry lining.

From the results of the analysis and interpretation of these data, in general, it can be stated that for the same values of flow discharge, channel bottom width, and channel bottom slope, the cross-sectional dimensions of GFRP material are more efficient than the cross-sectional dimensions of traditional materials (concrete and stone masonry). It can happen because the surface roughness of the GFRP material is smoother than the surface roughness of the concrete lining material and stone masonry lining material.

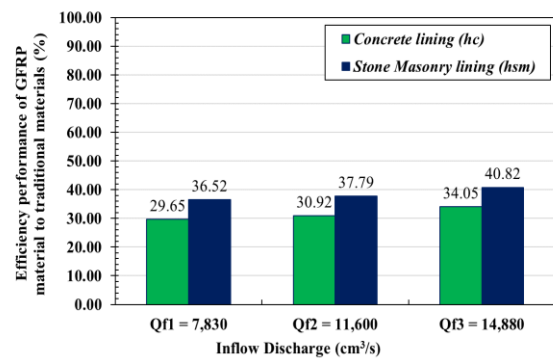


Figure 19. Comparative chart of the efficiency performance between the GFRP material and the traditional material (concrete and stone masonry) for three inflow variation discharge

4. CONCLUSION

From the results of the analysis and interpretation of the data between the physical modeling and the mathematical modeling, several conclusions can be written as follows:

1. Before the calibration process was carried out, the performance of the physical model already had "very good" results, where the results of the quantitative accuracy assessment using the Nash-Sutcliffe Efficiency (NSE) method gave a performance index for flow depth (h) between 0.881 and 0.910 and a performance index for flow velocity (v) is between 0.844 to 0.971. However, because there are relatively large deviation and anomaly values for the two flow parameters in several conditions of the channel bottom slope, the calibration process is still carried out by changing the value of the Manning roughness coefficient input in the mathematical modeling. The results of the re-simulation of water flow with the HEC-RAS software give more minor deviation results, and the graphic of the results of the comparison of the two flow parameters also looks smoother. The final value for the model performance index is also getting better, where the performance index for flow depths (h) are between 0.910 to 0.977, the performance index for flow velocities (v) are between 0.952 to 0.971, and the performance index for Manning roughness coefficients (n) are between 0.908 to 0.999.
2. By regulating three variations of inflow discharge in this experimental test, as the discharge (Q) increases, the flow depth (h) and flow velocity (v) also increase. By adjusting the nine variations of channel bottom slope in this experimental test, as the bottom slope (S) increases, the flow velocity (v) also increases, but the flow depth (h) decreases.
3. In subcritical flow conditions, the value of the Manning roughness coefficient (n) tends to be high and unstable. The value of the Manning roughness coefficient (n) tends to stabilize at supercritical flow.
4. From the results of this experimental test, the average Manning roughness coefficient (n) for low inflow discharge ($Q_{f1} = 7,830 \text{ cm}^3/\text{s}$) is 0.0083; for medium inflow discharge ($Q_{f2} = 11,600 \text{ cm}^3/\text{s}$) is 0.0082; for high inflow discharge ($Q_{f3} = 14,880 \text{ cm}^3/\text{s}$) is 0.0079; and overall, the average value of the Manning roughness coefficient (n) is 0.0081.
5. For the discharge, channel bottom width, and channel bottom slope with the same values, the cross-sectional dimensions of GFRP material ($n = 0.0081$) are more efficient than the cross-sectional dimensions of concrete material ($n = 0.0143$) and stone masonry material ($n = 0.0167$) where it can happen because the surface roughness of the GFRP material obtained from the results of this research is smoother than the surface roughness of the concrete material and the

stone masonry material.

6. For practical purposes in designing irrigation channels in Indonesia using GFRP material with a rigid type, it is recommended to use a Manning roughness coefficient value of $n = 0.0081$.

5. ACKNOWLEDGMENTS

The authors would like to thank Rita Irmawaty and Hasanuddin University academic staff and Suyudi Akbari Habibi, Arif Dhiaksa, and Haryo Istianto, who have contributed to providing the necessary resources and support for conducting this study.

6. REFERENCES

1. Umum DP. Standar Perencanaan Irigasi. Kriteria Perencanaan Jaringan Irigasi (KP-01). 1986.
2. Anas AV, Suriamihardja D, Pallu MS, Irfan UR. Sustainability analysis of mining management on construction material in Jeneberang River, South Sulawesi. *International Journal of Engineering Research & Technology (IJERT)*. 2013;2(12):191-5. <https://doi.org/10.17577/IJERTV2IS120193>
3. Mattamana BA, Varghese S, Kichu P. River sand inflow assessment and optimal sand mining policy development. *Int J Emergency Technol Adv. Eng.* 2013;3:305-17. https://www.ijetae.com/files/Volume3Issue3/IJETAE_0313_52.pdf
4. Tahir J, Barat U, editors. Kerusakan Lingkungan Akibat Penambangan Galian Golongan C di Polewali Mandar (Studi Kasus Sungai Mandar di Polewali). *Prosiding Seminar Nasional Biologi*, September; 2017.
5. Hasyim S, Salam N, Pallu MS, Maricar F, editors. Studi Kecepatan Aliran pada Saluran Terbuka dengan Dinding Glass Fiber Reinforced Polymer (GFRP). *Prosiding Seminar Nasional Teknik Sipil UMS*; 2023.
6. Morrison WR, Comer AI. Use of geomembranes in Bureau of Reclamation canals, reservoirs, and dam rehabilitation: Materials Engineering and Research Laboratory Group, Civil Engineering ...; 1995.
7. Swihart J, Haynes J. Canal-lining demonstration project year 10 final report: US Department of the Interior, Bureau of Reclamation, Denver Technical ...; 2002.
8. Stark T, Hynes J. Geomembranes for Canal Lining. *Geosynthetics* 2009. February 25-27 2009, Salt Lake City, Utah. 2009.
9. Morgado F, Lopes GJ, de Brito J, Feiteira J. Portuguese irrigation canals: lining solutions, anomalies, and rehabilitation. *Journal of performance of constructed facilities*. 2012;26(4):507-15. [https://doi.org/10.1061/\(asce\)cf.1943-5509.0000230](https://doi.org/10.1061/(asce)cf.1943-5509.0000230)
10. El-Menshawey O, El-Sissy A, El-Wazery M, Elsad R. Electrical and mechanical performance of hybrid and non-hybrid composites. *International Journal of Engineering, Transactions A: Basics*. 2019;32(4):580-6. <https://doi.org/10.5829/ije.2019.32.04a.16>
11. Jesthi D, Nayak A, Routara B, Nayak R. Evaluation of mechanical and tribological properties of glass/carbon fiber reinforced polymer hybrid composite. *International Journal of Engineering, Transactions A: Basics*. 2018;31(7):1088-94. <https://doi.org/10.5829/ije.2018.31.07a.12>
12. Anish Jafrin Thilak J, Suresh P. Dynamic Response of Glass/Epoxy Laminated Composite Plates under Low-velocity

- Impact. *International Journal of Engineering*. 2022;35(7):1283-90. <https://doi.org/10.5829/ije.2022.35.07a.07>
13. Masuelli MA. Introduction of fibre-reinforced polymers–polymers and composites: concepts, properties and processes. Fiber reinforced polymers-the technology applied for concrete repair: IntechOpen; 2013.
 14. Estrada H, Lee LS. FRP composite constituent materials. *The International Handbook of FRP Composites in Civil Engineering*. 2014:31-2. <https://doi.org/10.1201/b15806-5>
 15. Haj Seiyed Taghia SA, Darvishvand HR, Pourhasan M. An Economic Approach to the Confinement of Different Concrete Classes with Carbon and Glass Fibers Reinforced Polymers. *International Journal of Engineering, Transactions A: Basics*. 2023;36(4):776-87. <https://doi.org/10.5829/ije.2023.36.04a.14>
 16. Zanelidin B. Fiber reinforced polymer materials in construction applications. *J Civ Eng Sci*. 2012;1(4):47-51. <http://paper.academicpub.org/Paper?id=1397>
 17. Mekonnen B, Mamo Y. Tensile and flexural analysis of a hybrid bamboo/jute fiber-reinforced composite with polyester matrix as a sustainable green material for wind turbine blades. *International Journal of Engineering, Transactions A: Basics*. 2020;33(2):314-9. <https://doi.org/10.5829/ije.2020.33.02b.16>
 18. El-Wazery M. Mechanical characterization of glass-basalt-carbon/polyester hybrid composites. *International Journal of Engineering, Transactions A: Basics*. 2018;31(7):1139-45. <https://doi.org/10.5829/ije.2018.31.07a.19>
 19. Prasanth I, Ravishankar D, Manzoor Hussain M. Analysis of milling process parameters and their influence on glass fiber reinforced polymer composites (research note). *International Journal of Engineering, Transactions A: Basics*. 2017;30(7):1074-80. <https://doi.org/10.5829/ije.2017.30.07a.17>
 20. Pang L. Fiberglass Reinforced Polyester Flumes as Tertiary Channels in Malaysian Irrigation Development: *International Rice Research Institute*; 1978.
 21. Okazawa H, Takeuchi Y, Mashino M, Maki T. Coefficient of roughness at an open channel repaired with flexible fiber-reinforced plastic lining. *Journal of Agriculture Science, Tokyo University of Agriculture (Japan)*. 2008;53(3). https://www.nntechinfo.jp/NNTD/files/0324/0324_1102.pdf
 22. Chow VT. A note on the Manning formula. *Eos, Transactions American Geophysical Union*. 1955;36(4):688-. <https://doi.org/10.1029/TR036i004p00688>
 23. Manning R, Griffith JP, Pigot T, Vernon-Harcourt LF. On the flow of water in open channels and pipes 1890.
 24. Mera M, Robi R. Technical Notes: Determination of Manning Roughness Coefficient for PVC Gutters. *Jurnal Teknik Sipil ITB*. 2013;20(2):153-60. <https://doi.org/10.5614/jts.2013.20.2.8>
 25. Brunner GW, editor *Hec-ras (river analysis system)*. North American water and environment congress & destructive water; 2002: ASCE.
 26. Te Chow V. *Open channel hydraulics* 1959.
 27. Moriasi DN, Arnold JG, Van Liew MW, Bingner RL, Harmel RD, Veith TL. Model evaluation guidelines for systematic quantification of accuracy in watershed simulations. *Transactions of the ASABE*. 2007;50(3):885-900. <https://doi.org/10.13031/2013.23153>
 28. Legates DR, McCabe Jr GJ. Evaluating the use of “goodness-of-fit” measures in hydrologic and hydroclimatic model validation. *Water resources research*. 1999;35(1):233-41. <https://doi.org/10.1029/1998WR900018>
 29. ASCE Task Committee on Definition of Criteria for Evaluation of Watershed Models of the Watershed Management Committee I, Division D. Criteria for evaluation of watershed models. *Journal of Irrigation and Drainage Engineering*. 1993;119(3):429-42. [https://doi.org/10.1061/\(ASCE\)0733-9437\(1993\)119:3\(429\)](https://doi.org/10.1061/(ASCE)0733-9437(1993)119:3(429))
 30. Singh J, Knapp HV, Arnold J, Demissie M. Hydrological modeling of the Iroquois river watershed using HSPF and SWAT 1. *JAWRA Journal of the American Water Resources Association*. 2005;41(2):343-60. <https://doi.org/10.1111/j.1752-1688.2005.tb03740.x>
 31. Nash JE, Sutcliffe JV. River flow forecasting through conceptual models part I—A discussion of principles. *Journal of hydrology*. 1970;10(3):282-90. [https://doi.org/10.1016/0022-1694\(70\)90255-6](https://doi.org/10.1016/0022-1694(70)90255-6)
 32. Van Liew M, Arnold J, Garbrecht J. Hydrologic simulation on agricultural watersheds: Choosing between two models. *Transactions of the ASAE*. 2003;46(6):1539-51. <https://doi.org/10.13031/2013.15643>

COPYRIGHTS

©2024 The author(s). This is an open access article distributed under the terms of the Creative Commons Attribution (CC BY 4.0), which permits unrestricted use, distribution, and reproduction in any medium, as long as the original authors and source are cited. No permission is required from the authors or the publishers.

**Persian Abstract****چکیده**

یکی از تلاش‌ها برای کاهش تلفات آب در کانال‌های آبیاری، تامین مواد آستردهار در کانال‌های آبیاری زمین است. ساخت این مواد آستردهار در اندونزی به مواد خام (مانند شن، ماسه و سنگ شکافی) نیاز دارد که از طبیعت استخراج می‌شود و در اندونزی که به عنوان مواد حفاری کلاس C شناخته می‌شود. بهره برداری بیش از حد از مواد حفاری کلاس C بر آسیب‌های زیست محیطی تأثیر می‌گذارد. بنابراین برای غلبه بر این مشکلات، تحقیقاتی برای یافتن مواد پوشش‌دار جایگزین مورد نیاز است و در این تحقیق، ماده پوشش‌دهنده جایگزین پلیمر تقویت‌شده با الیاف شیشه (GFRP) است. هدف اصلی این مطالعه تعیین مقدار ضریب زبری مانینگ برای کانال‌های اندود شده از مواد GFRP بود. این تحقیق شامل آزمایش تجربی با استفاده از مدل کانال باز (فلوم) پوشیده شده با مواد GFRP بود. آزمایش‌های جریان با سه تغییر دبی جریان پمپ و نه تغییر شیب پایین کانال انجام شد. نتایج آزمون مدل فیزیکی با نتایج شبیه‌سازی مدل ریاضی با استفاده از نرم‌افزار HEC-RAS مقایسه شد. عملکرد مدل با استفاده از تکنیک گرافیکی و آمار کمی به ویژه روش کارایی نش-ساتکلیف (NSE) مورد ارزیابی قرار گرفت. ارزیابی مدل با روش NSE نشان می‌دهد که عملکرد مدل فیزیکی "بسیار خوب" است. مقدار ضریب زبری Manning برای مواد GFRP با روکش صلب از 0.0071 تا 0.0102 متغیر است. مقدار ضریب زبری مانینگ توصیه شده برای کاربرد عملی در طراحی کانال‌های آبیاری در اندونزی 0/0081 است.